ELSEVIER

Catalysis Today 43 (1998) 147–158

CATALYSIS TODAY

NEXAFS determination of electronic and catalytic properties of transition metal carbides and nitrides: From single crystal surfaces to powder catalysts

J.G. Chen*, J. Eng Jr., S.P. Kelty[1]

Corporate Research Laboratories, Exxon Research and Engineering Company, Annandale, NJ 08801, USA

Abstract

In this paper we will provide a brief review of our recent investigations of the physical and chemical properties of transition metal carbides and nitrides using the near-edge X-ray absorption fine structure (NEXAFS) technique. We will first use single crystal model surfaces to demonstrate the capabilities of NEXAFS for determining fundamental electronic and structural properties of transition metal carbides and nitrides, such as the ionicity of the metal–nonmetal bonds, the *p*-projected density of unoccupied states, and the location of carbon and nitrogen atoms on the surface or interstitial subsurface sites. We will use several examples to correlate these electronic and structural properties to the chemical reactivities of the transition metal carbide and nitride model surfaces. Furthermore, we will compare the general similarities of the NEXAFS investigations between model surfaces and powder catalysts. We will also provide several examples to demonstrate how the fundamental learnings from the model surfaces can be used to understand the catalytic properties of powder materials with complicated catalytic formulations, such as the bimetallic oxycarbide and oxynitride catalysts.

1. Introduction

Ever since the landmark paper by Levy and Boudart regarding the Pt-like properties of tungsten carbides [1], the catalytic properties of transition metal carbides (TMC) and nitrides (TMN) have been the subject of numerous experimental and theoretical investigations. It is now well established that, compared to their parent metals, TMC and TMN often demonstrate catalytic advantages in activity, selectivity, and resistance to poisoning. It has also been demonstrated in many studies that the catalytic performances of TMC and TMN are similar to those of the more expensive Pt-Group metals (Pt, Pd, Ir, Rh and Ru), particularly in catalytic reactions involving the transformation of C–H bonds of hydrocarbons, such as in dehydrogenation, hydrogenation, hydrogenolysis, and isomerization reactions. Furthermore, TMC and TMN also have a potential catalytic advantage over Pt-group metals because of their higher sulfur and nitrogen tolerance. More detailed discussions concerning the catalytic properties of TMC and TMN can be found in several recent reviews [2–4].

In the past few years we have performed a series of surface science investigations in an attempt to understand primarily two fundamental questions regarding the unique catalytic properties of TMC and TMN: (a) why are the chemical properties of TMC and TMN

*Corresponding author. E-mail: jchen@erenj.com

[1]Current Address: Department of Chemistry, Seton Hall University, South Orange, NJ 07079.

0920-5861/98/$32.00
PII S0920-5861(98)00143-6

different from those of their parent metals and (b) what are the underlying electronic and structural factors that are responsible for the general similarities between Pt-group metals and certain TMC and TMN catalysts? To answer these questions we have adopted three parallel experimental approaches: (1) to develop experimental procedures for the preparation of thin TMC and TMN films with desired electronic and structural properties; (2) to compare the surface reactivities of the model TMC and TMN thin films to those of the Pt-group metals; and (3) to correlate the chemical reactivities of model surfaces to the catalytic properties of powder catalysts by the utilization of the near-edge X-ray absorption fine structure (NEXAFS) technique. We have summarized the first two aspects of our surface science studies in two recent reviews [4,5]; in this paper we will review briefly our NEXAFS studies of the electronic, structural, and catalytic properties of TMC and TMN in the form of both model surfaces and powder catalysts. We will choose several of our NEXAFS studies of TMC and TMN surfaces and catalysts as examples to provide a systematic overview of the basic principles, experimental approaches, and unique advantages of the NEXAFS measurements. These examples include both previously published results and some more recent measurements.

It is important to point out that the electronic, structural, and catalytic properties of TMC and TMN have been investigated by many other research groups using a variety of experimental techniques. These studies have been discussed extensively in several general reviews concerning the physical and chemical properties of TMC and TMN [2–4]. In the current paper we will concentrate on results from our own laboratory, particularly on the utilization of NEXAFS to determine the electronic and catalytic properties of TMC and TMN.

The rest of this paper is organized as follows: In Section 2 we will briefly discuss the experimental set-up and procedures for performing NEXAFS measurements. In Section 3 we will provide an overview of the general correlation between the near-edge features and the electronic and structural properties of TMC and TMN. In Section 4 we will demonstrate the utilization of NEXAFS for understanding the unique chemical reactivities of several TMC and TMN model surfaces. In Section 5 we will discuss the application of NEXAFS to monometallic and bimetallic carbide and nitride powder catalysts. Finally, in Section 6 we will provide a summary of the main advantages of the NEXAFS technique for determining the electronic and catalytic properties of TMC and TMN.

2. Experimental

The NEXAFS measurements reported here were performed at the U1A Beamline of the National Synchrotron Light Source, Brookhaven National Laboratory. The experimental end-station is equipped with capabilities to measure both single crystal surfaces [6] and powder materials [7]. The NEXAFS spectra were recorded by measuring either the surface-sensitive partial electron-yield or the bulk-sensitive fluorescence-yield signals [8,9]. Details about the beamline optics and NEXAFS detectors have been described previously [9,10].

Thin films of TMC can be obtained typically by exposing the parent transition metal surfaces to unsaturated hydrocarbon molecules at elevated temperatures; TMN overlayers can be prepared by reacting the parent metal surfaces with either N_2 or ammonia. Surface structures and the metal/non-metal stoichiometries are typically determined by using low energy electron diffraction (LEED) and Auger electron spectroscopy (AES), respectively. Details about the preparation and characterization of various TMC and TMN surfaces can be found elsewhere [4].

Samples of powder TMC and TMN materials are first ground to fine powders and then pressed into stainless steel sample holders. The powder samples readily react with air, during either the sample preparation or sample transfer, to produce a surface oxide layer. Oxygen impurities typically can be removed by heating the TMC and TMN samples ($T \geq 700$ K) in 10–50 Torr of H_2 prior to NEXAFS measurements [11].

3. Overview of NEXAFS studies of TMC and TMN

3.1. *Information from the K-edge features of carbon and nitrogen*

The left panel of Fig. 1 shows the C K-edge spectrum of TiC and the N K-edge spectrum of TiN. For

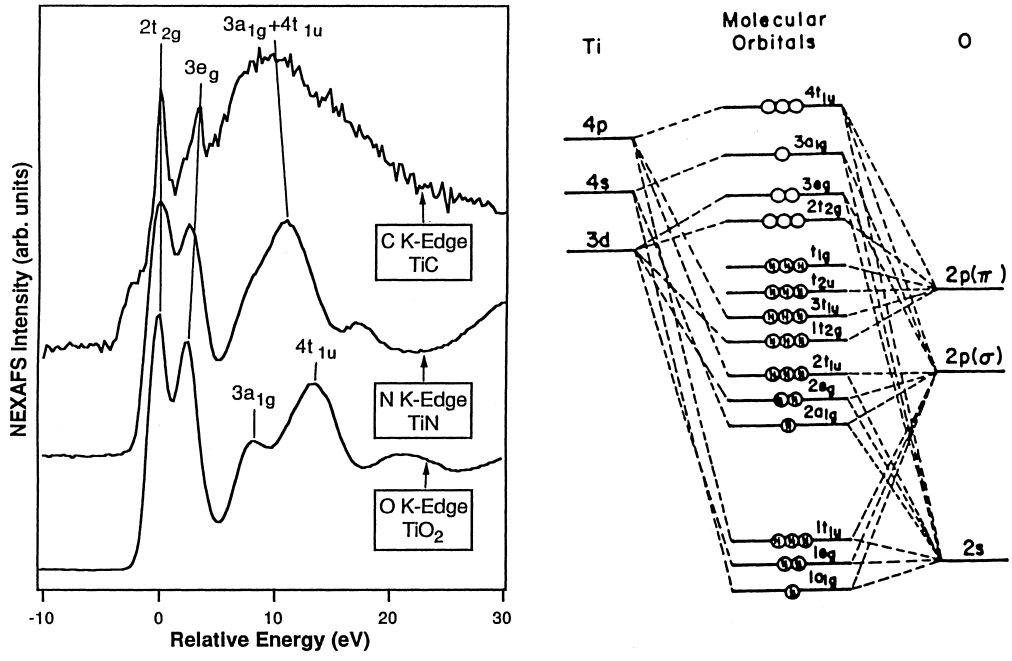

Fig. 1. Left panel: A comparison of K-edge features of TiO_2 (anatase), TiN and TiC powder materials. For ease of comparison the t_{2g} peaks of the three K-edge spectra are normalized to the same energy position. Right panel: A molecular orbital diagram of a $(TiO_6)^{8-}$ ion cluster in an octahedral symmetry (after Fischer [12]). The orbital diagram was obtained from a symmetry-determined molecular orbital model using the linear combination of atomic orbital (LCAO) method.

comparison, the O K-edge spectrum of an anatase TiO_2 sample is also included in Fig. 1. The spectroscopic assignment of the O K-edge features of TiO_2 can be accomplished by using an empirical, symmetry-determined molecular orbital model which involves the transition of an O 1s electron to the various partially occupied and unoccupied molecular orbitals of TiO_2. This rather simple molecular orbital model was first proposed by Fischer for TiO_2 [12], and was later applied to other transition metal oxides by others [13–15]. As shown in the orbital diagram in the right panel of Fig. 1 for a $(TiO_6)^{8-}$ ion cluster, which represents TiO_2 in an octahedral symmetry, TiO_2 has four unoccupied molecular orbitals in the energetic order of $2t_{2g}$ (Ti 3d+O 2pπ)<$3e_g$ (Ti 3d+O 2pσ)<$3a_{1g}$ (Ti 4s+O 2pσ)<$4t_{1u}$ (Ti 4p+O 2pπ). The atomic orbitals listed in parentheses are those that contribute dominantly to the corresponding hybridized molecular orbitals. As labeled in Fig. 1, the first four relatively intense O K-edge features of anatase TiO_2 have been assigned according to the excitation of the O 1s electron to these four molecular orbitals.

The C and N atoms in TiC and TiN (rock salt structure) also have the octahedral bonding configuration, which should lead to a similar molecular orbital diagram to that of TiO_2. One minor difference is that the oxidation state of Ti in TiC and TiN should be different from that of Ti^{4+} (d^0 electronic configuration) in TiO_2. However, the number of *d*-electrons in TiC and TiN is not sufficient to completely fill the three $2t_{2g}$ orbitals. As a result, both TiC and TiN should have the same four types of partially-occupied or unoccupied orbitals. This is confirmed experimentally by the general similarity in the C, N, and O K-edge spectra shown in Fig. 1. Similar to the assignment discussed for TiO_2, the first two relatively sharp features in TiC and TiN can be assigned to the $2t_{2g}$(Ti 3d+C or N 2pπ) and $3e_g$ (Ti 3d+C or N 2pσ) orbitals, respectively. In addition, the $3a_{1g}$ and $4t_{1u}$ orbitals, resulting from the hybridization of Ti 4sp and C or N 2p states, are no longer well-resolved and appear as one broad peak in TiC or TiN.

The NEXAFS studies measure dipole transitions that are governed by the dipole selection rule which

states that the change in the angular momentum quantum number (Δl) is ± 1. For the K-edge features of carbon and nitrogen, which results from the excitation of an 1s electron, the dipole selection rule requires that the final states must have contributions from the *p*-type orbitals. Therefore, to a first approximation, the K-edge spectrum of carbon or nitrogen can be envisioned as a direct image of the *p*-projected unoccupied density of states (DOS). Furthermore, the number of unoccupied orbitals and their energy positions are determined by the symmetry of the carbides or nitrides. As a result, the C and N K-edge spectra, such as those shown in Fig. 1, provide important information about the electronic and structural properties of the corresponding TMC and TMN compounds. For example, the overall similarities of the K-edge spectra of TiC and TiN in Fig. 1 confirm the similar crystal structures and local bonding environment of the two compounds. In addition, NEXAFS is also very sensitive to minor differences in the electronic properties. For example, a more detailed comparison of the NEXAFS spectra of TiC and TiN reveals some minor differences between the two compounds. The comparison indicates that the degree of overlapping between the Ti 3*d* and the non-metal 2*p* orbitals, which is reflected by the value of the ligand-field splitting, $\Delta E(2t_{2g}-3e_g)$ [9,13], increases from TiN to TiC. On the other hand, the comparison also suggests that the degree of interaction between the Ti 4sp and the non-metal 2*p* orbitals, which is related to the energy separation between the $2t_{2g}$ and the $(3a_{1g}+4t_{1u})$ orbitals [9,13], decreases from TiN to TiC. More about the correlation between the K-edge features of the 2*p* elements and the properties of the corresponding transition metal compounds can be found in a recent review [9].

3.2. *Information from the near-edge features of parent metals*

The near-edge features of the parent metals in TMC and TMN often provide additional or complementary information to the K-edge features of carbon and nitrogen. One important example is the determination of the oxidation state of the parent metal in TMC and TMN. The left panel of Fig. 2 shows NEXAFS measurements of Mo M_{III} and M_{II} near-edge features, which involve the transition of $3p_{3/2}$ and $3p_{1/2}$ electrons, respectively, to unoccupied 4*d* orbitals. As shown in the right panel of Fig. 2, the peak center of the M_{III} feature increases nearly linearly from metallic Mo to MoO_2 (Mo^{4+}) and MoO_3(Mo^{6+}). Such a relationship can be used to determine the oxidation state of Mo in carbides or nitrides. For example, based on the position of the M_{III} feature, the Mo oxidation state for a thin carbide film on Mo(110) is determined to be approximately $Mo^{0.2+}$. This observation suggests that there is very little charge transfer between Mo and C, and that the Mo–C bonding is mainly covalent. It is important to point out that such covalent bonding does not occur for all TMC. For example, the oxidation state of vanadium in a thin carbide film on V(110) has been studied by comparing the V L-edge ($2p\rightarrow 3d$) peak positions with those of several vanadium oxides. These studies found that the oxidation state of V in the carbide overlayer is $V^{1.2+}$, indicating a very significant contribution of ionic bonding in the V–C bonds [16,17].

In addition, the spectral shape of the metal L-edge (for 3*d* compounds) or M-edge (for 4*d* compounds) features are related to the density of states (DOS) of the unoccupied *d*-orbitals. In a comparative study of the V L-edge features of metallic V and VC, the peak widths of the V L-edge features of VC were found to be much broader than those of V. Such a broadening in the DOS of the unoccupied *d*-orbitals of VC has been proposed as one of the contributing factors for the enhanced activity in the dissociation of the C–H bonds of alkanes on VC surfaces [18,19].

4. Examples of NEXAFS studies of TMC and TMN model surfaces

4.1. *Comparison of electronic properties of C/Mo(110) and C/V(110)*

We have performed detailed comparative studies, using the clean and carbide-modified Mo(110) surfaces as model systems, to understand how the formation of a carbide overlayer modifies the surface reactivity of an early transition metal such as molybdenum. Using a variety of surface science techniques [4,5], we have compared the different reactivities of a number of inorganic and organic probing molecules, including CO [20], ethylene [21], 2-butenes [22],

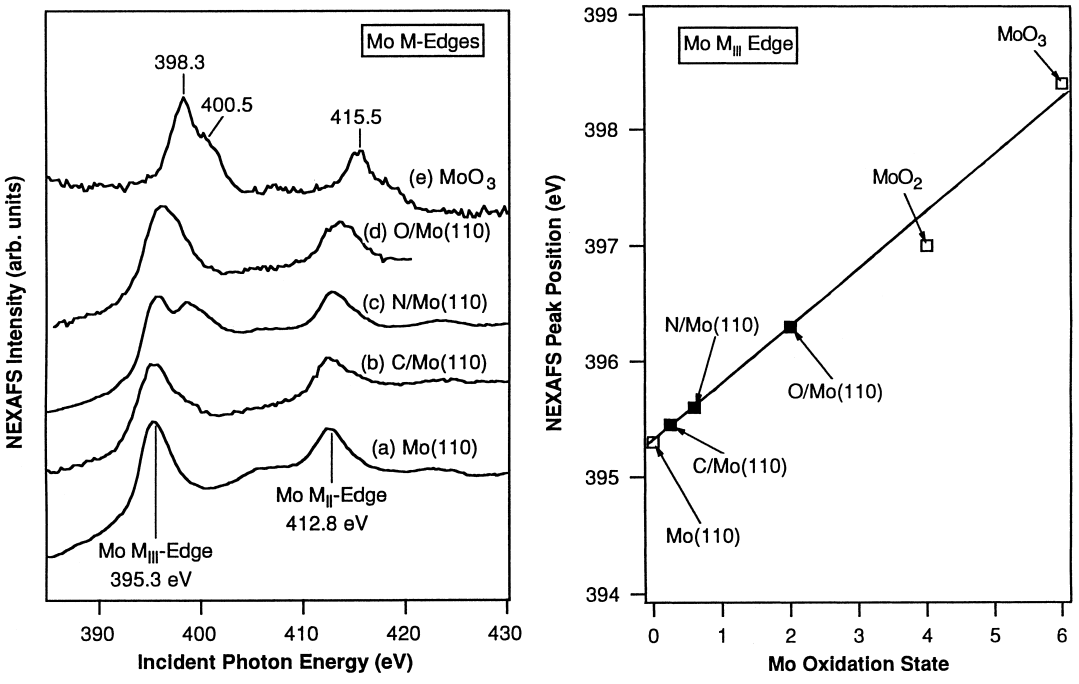

Fig. 2. Left panel: A comparison of Mo M-edge spectra of a Mo(110) surface with C/Mo(110), N/Mo(110), O/Mo(110), and a MoO_3 powder sample; the NEXAFS spectra were recorded by measuring the partial electron yield. The C/Mo(110) surface was prepared by repeated cycles of exposing Mo(110) to ethylene at 600 K followed by annealing to 1200 K; the N/Mo(110) layer was prepared by exposing Mo(110) to 300 L N_2 at 600 K; the O/Mo(110) was obtained by exposing Mo(110) to 100 L O_2 at 1000 K. The additional feature in the M_{III} region of N/Mo(110) is due to a N K-edge feature. Right panel: A comparison of the M_{III} peak center as a function of the Mo oxidation state in Mo(110), MoO_2 and MoO_3. The Mo M_{III} peak centers of C/Mo(110), N/Mo(110), and O/Mo(110) are also included for determining the Mo oxidation state in these overlayers.

cyclohexene [23], cyclohexadiene [24] and benzene [25]. In all these studies we found that the high reactivity of Mo(110) can be 'tamed' by the formation of carbide. Furthermore, we found that the reaction pathways of these probing molecules on the carbide-modified Mo(110) surface are very similar to those typically observed on the Pt-group metals, as long as the C/Mo(110) overlayer is characterized by an interstitial carbide structure [4]. The latter subject will be discussed further in Section 4.2.

In addition, we have also observed similar Pt-like properties for the carbide-modified V(110) surface, as judged by the formation of the characteristic ethylidyne (CCH_3) species from the decomposition of ethylene [26,27]. However, carbide-modified V(110) and Mo(110) surfaces show very different reactivities towards the activation of the C–H bonds, particularly the C–H bonds of alkanes [4]. We have performed comparative NEXAFS investigations of the two carbide-modified surfaces, which revealed two major differences in the electronic properties of C/V(110) and C/Mo(110). First, as discussed in Section 3.2, the V–C bonds are much more ionic than the Mo–C bonds, as determined from the peak positions of the V L-edge and Mo M-edge features. Second, the *p*-projected DOS of the unoccupied orbitals of C/V(110) and C/Mo(110) is also different, which is illustrated in the C K-edge spectra shown in Fig. 3. The C K-edge regions of the carbide overlayers on both V(110) and Mo(110) are characterized by the typical three-peak spectra of early transition metal carbides; the assignment of the three features is similar to that discussed earlier for TiC in Fig. 1. However, the relative intensities and line shape of these features are significantly different between C/V(110) and C/Mo(110), reflecting the differences in the DOS of the corresponding molecular orbitals. The differences in the ionicity and the *p*-projected DOS could be responsible for

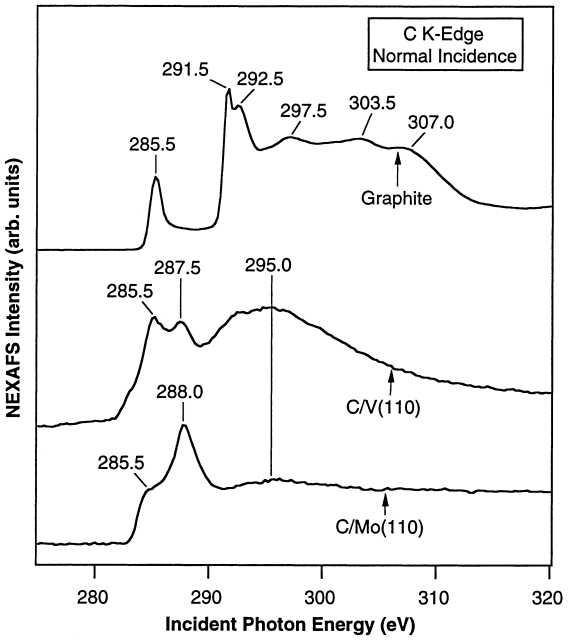

Fig. 3. A comparison of C K-edge spectra of carbide overlayers prepared on Mo(110) and V(110); the NEXAFS spectra were recorded by measuring the partial electron yield. The C/Mo(110) surface was prepared by repeated cycles of exposing Mo(110) to ethylene at 600 K followed by annealing to 1200 K; the C/V(110) layer was obtained after exposing V(110) to 1000 L ethylene at 600 K [16]. The K-edge spectrum of a polycrystalline graphite sample is also included for comparison.

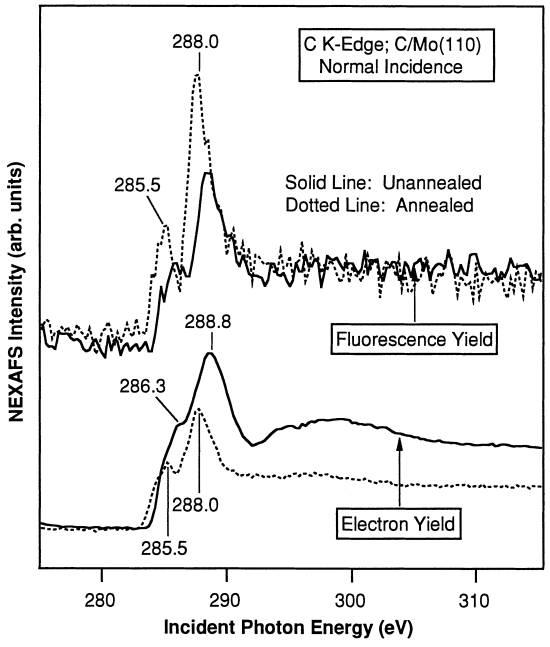

Fig. 4. A comparison of C K-edge features of C/Mo(110) recorded before (solid line) and after (dotted line) annealing to 1200 K. The spectra at the lower and upper parts of Fig. 3 are from measuring the surface sensitive partial electron yield and the bulk-sensitive fluorescence yield signals, respectively (from [29]).

the different reactivities of the C/V(110) and C/Mo(110) surfaces [4].

Furthermore, Fig. 3 also shows that the C K-edge features of TMC are qualitatively different from those of graphite. They are also very different from the C K-edge features of other forms of carbon, such as diamond, fullerenes, and amorphous carbon films [9]. As a result, the typical three-peak C K-edge features can be used as characteristic 'fingerprints' for the presence of carbide in a mixture containing other forms of solid carbon materials.

4.2. *Comparison of thermal stability of C/Mo(110) and C/Ni(111)*

In order to understand the thermal stability of various TMC, we have studied the thermal behavior of carbide overlayers on a number of closely packed transition metal surfaces, including Ti(0001), V(110), Mo(110), Fe(110), Co(0001), and Ni(111). We found that the carbide films on early transitions metal surfaces are much more stable than those on late transition metals. Our comparative NEXAFS studies of the thermal stability of C/Mo(110) and C/Ni(110) have provided important information about thermally induced structural changes, as well as their effects on the chemical reactivities of the carbide overlayers, on early and late transition metal surfaces.

Fig. 4 shows a comparison of NEXAFS spectra recorded before and after heating a C/Mo(110) overlayer to 1200 K; the C/Mo(110) overlayer was prepared by exposing a clean Mo(110) surface to 300 L (1 L=1×10^{-6} Torr·s) ethylene at 300 K [29]. The bottom two NEXAFS spectra were collected using the surface-sensitive partial electron yield method [9]. A comparison of the two spectra shows that the peak positions of the first two carbon K-edge features are slightly shifted, from 286.3 and 288.8 eV before annealing to 285.5 to 288.0 eV after annealing. However, the overall line shape and peak positions of the two C K-edge spectra remain characteristic of TMC,

indicating that the molybdenum carbide overlayer is thermally stable up to 1200 K.

Fig. 4 also shows the importance of measuring NEXAFS spectra using both the surface-sensitive electron yield and the bulk-sensitive fluorescence yield spectra methods. For example, changes in the carbon concentration, from before and after annealing the C/Mo(110) overlayer, can be determined from the height of the edge jump in the C K-edge features [8,9]. While the electron yield NEXAFS spectra show a decrease in the edge jump after annealing the carbide overlayer to 1200 K, the height of the edge jump in the fluorescence yield spectra remains nearly constant before and after annealing. This difference is related to the different detection limits of the two methods; the mean-free paths of the Auger electrons and photons in the C K-edge region are approximately 10 Å and 1500 Å, respectively [8,9]. The comparison of the electron yield and fluorescence yield NEXAFS results in Fig. 4, combined with results from other surface spectroscopies, allowed us to conclude that annealing the C/Mo(110) surface to 1200 K induces the diffusion of carbon from the top most surface layer to the subsurface interstitial sites. This diffusion model explains the different chemical reactivities of the unannealed (600 K) and annealed (1200 K) C/Mo(110) surfaces [28,29]. For example, the unannealed C/Mo(110) surface is chemically inert due to the fact that the surface-active sites are occupied by carbon atoms. In contrast, the annealed carbide overlayer is characterized by Pt-like reactivities, indicating that the Pt-like properties can only be achieved after the formation of an interstitial carbide overlayer [29].

On the other hand, carbide overlayers on late transition metal surfaces are much less stable at high temperatures. Fig. 5 shows a comparison of the C K-edge spectra of a C/Ni(111) overlayer before and after heating the surface to 900 K; the carbide overlayer was prepared by exposing ethylene to an epitaxial Ni(111) thin film at 600 K [30]. The C/Ni(111) surface at 600 K has the characteristic C K-edge features of TMC, which disappear after the C/Ni(111) surface is heated at 900 K. The top two spectra in Fig. 5 were recorded with the angles of the incident photons at normal and 25° glancing with respect to the Ni(111) surface. The overall C K-edge features in the two spectra are similar to those of the polycrystalline graphite shown in Fig. 3. One notable

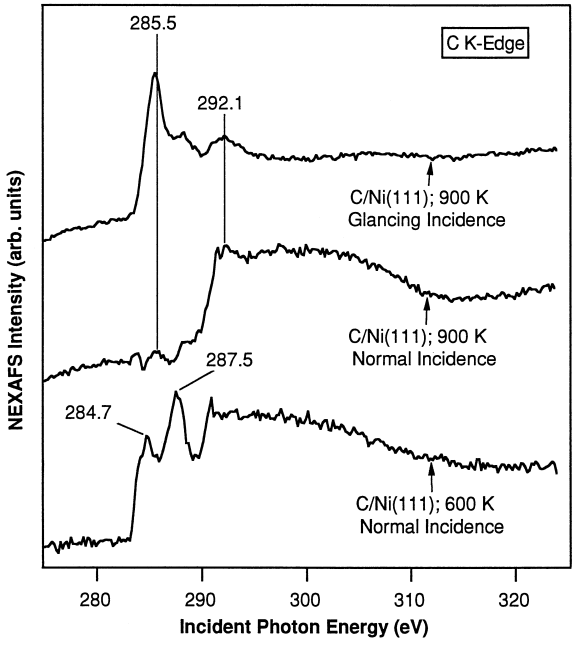

Fig. 5. A comparison of the C K-edge spectra of C/Ni(111) before and after heating the surface to 900 K; the NEXAFS spectra were recorded by measuring the partial electron yield. The NEXAFS spectrum of the 600 K carbidic C/Ni(111) was recorded with the incident photon beam normal to the Ni(111) surface. The spectra of the 900 K graphitic C/Ni(111) surface was recorded at both normal and glancing incidence to reveal the orientation of the graphite overlayer.

exception is that the intensities of the C K-edge features of graphite on Ni(111) are dependent on the angles of the incident photons, with the π^* feature at 285.5 eV being very intense at the glancing incidence and the σ^* features at ~292.1 eV at higher energies being more intense at the normal incidence. Such an angular dependence suggests that the carbidic carbon atoms on Ni(111) are converted to graphite at 900 K, and that the basal plane of graphite is parallel to the Ni(111) surface [8]. The NEXAFS detection of the thermally induced conversion of carbide to graphite on Ni(111) helps to explain the different reactivities of the carbidic (600 K) and graphitic (900 K) C/Ni(111) surfaces [5,30]. For example, using the dehydrogenation of cyclohexene as a probing reaction, a Pt-like reactivity is observed for the carbidic C/N(111) surface. Such a Pt-like reactivity disappears after the surface is annealed to 900 K, indicating clearly that the carbidic and graphitic carbon atoms

modify the surface reactivities of Ni in a qualitatively different manner.

4.3. Determination of binding sites in N/Mo(110)

The polarization-dependence NEXAFS measurements, such as that shown in Fig. 5 for the investigation of graphite on Ni(111), can also be used to determine the binding sites of carbon and nitrogen in the TMC and TMN overlayers. For example, after exposing a Mo(110) surface to nitrogen or ammonia at a temperature range of 600–800 K, the N/Mo(110) surface was found to be chemically inert towards the decomposition of unsaturated hydrocarbons [23,29]. One possible explanation is that, instead of producing a bulk-like molybdenum nitride overlayer, nitrogen atoms only occupy the surface sites of Mo(110). The presence of surface nitrogen atoms prevents the chemisorption and subsequent reaction of hydrocarbons on the N/Mo(110) surface, either via a site-blocking [29] or an electronic modification [31,32] of the Mo surface. The presence of surface nitrogen atoms is confirmed by the polarization dependence NEXAFS studies of N/Mo(110), as shown in Fig. 6. Due to the face-centered-cubic (fcc) crystal structure of bulk molybdenum nitride, the overall angular distribution of the Mo–N bonds in a bulk-like nitride overlayer should be isotropic. As a result, the N K-edge spectra of a bulk-like nitride overlayer should be identical in the normal and glancing incidence measurements [9]. On the other hand, if N atoms occupy the surface sites only, the angular distribution of the Mo–N bonds is no longer isotropic. One should then expect to observe an angular dependence of the N K-edge features. The comparison in Fig. 6 clearly indicates that the peak position and the line shape of the N K-edge features are strongly dependent on the polarization of the incident photons, supporting the argument that the nitrogen atoms occupy only the surface sites on Mo(110) [29].

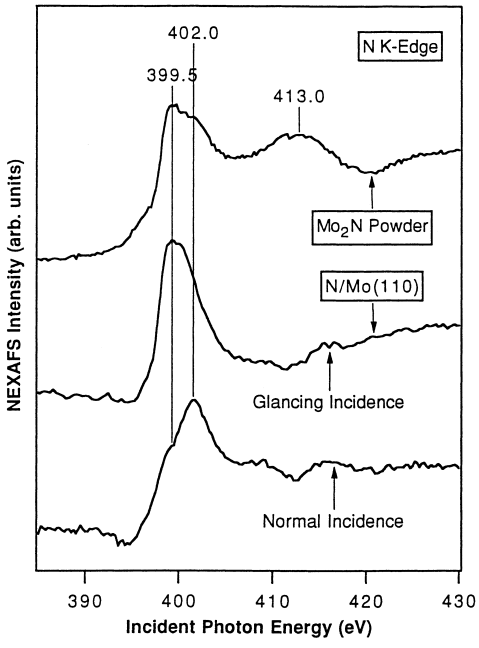

Fig. 6. A comparison of a N/Mo(110) surface recorded at normal and glancing incidence; the NEXAFS spectra were recorded by measuring the partial electron yield. The strong angular dependence of the N K-edge features on Mo(110) is related to the adsorption of N on the surface sites instead of in the interstitial subsurface sites. The N K-edge features from a Mo_2N powder sample is also included for comparison.

5. Examples of NEXAFS studies of TMC and TMN powder catalysts

5.1. Comparison of model surfaces with bulk and supported catalysts

In order to correlate the fundamental learnings from model surfaces to powder catalysts, we have performed a series of comparative NEXAFS investigations of the two classes of materials. In general, we found strong similarities in the NEXAFS spectra between the model surfaces and powder materials. For example, both the C K-edge and V L-edge spectra of the C/V(110) surface are essentially identical to those of VC powder catalysts [19]; similar results are also observed in the NEXAFS comparison of C/Mo(110) with Mo_2C powder materials [5].

We have also compared the C K-edge features of bulk Mo_2C [5], molybdenum oxycarbides (Mo_2C-O) [5], and Mo_2C supported on alumina [33]. The NEXAFS results provided important information about the similarities and differences between the three catalysts. For example, as judged from their C K-edge spectra, all three powder catalysts retain their carbidic nature. However, the relative intensities and peak

positions of the C K-edge features of the Mo_2C–O and supported Mo_2C catalysts are notably different from those of either C/Mo(110) or bulk Mo_2C [5,33], suggesting that the electronic and structural properties of these catalysts are modified due to the interaction of Mo_2C either with the interstitial oxygen (in Mo_2C–O) or with alumina (in supported carbides). Another observation is that the concentration of graphite at or near the surface region, as determined from the relative intensities of the graphite C K-edge features in the electron yield NEXAFS measurements, is typically less in Mo_2C–O and supported Mo_2C catalysts than in bulk Mo_2C [5]. These NEXAFS results help to explain the different catalytic activities of Mo_2C–O and supported Mo_2C catalysts as compared to those of the unsupported bulk Mo_2C [33].

5.2. *Characterization of bimetallic oxycarbides and oxynitrides*

We have also applied NEXAFS to determine the electronic and catalytic properties of more complicated TMC and TMN systems, such as the so-called bimetallic oxycarbide and bimetallic oxynitride catalysts [34,35]. Fig. 7 shows the C K-edge spectra of several Nb–Mo bimetallic oxycarbides, which are compared to the C K-edge features of the corresponding monometallic oxycarbides, NbC–O and Mo_2C–O [34]. The comparison of the C K-edge spectra in Fig. 7 reveals the following similarities and differences between the three Nb–Mo oxycarbide catalysts: (1) The characteristic carbide K-edge features are observed in all NEXAFS spectra, indicating the presence of carbidic carbon in all three bimetallic oxycarbides. (2) Among the three oxycarbides, the $Nb_{1.0}Mo_{2.0}$–O–C catalyst shows a pronounced feature at 292.5 eV, demonstrating the presence of graphite at or near the surface region. (3) The step height of the C K-edge spectrum of $Nb_{1.0}Mo_{0.67}$–O–C, which is related to the total carbon concentration near the surface region, is only about 75% that of the other two catalysts, suggesting a carbon deficiency in the $Nb_{1.0}Mo_{0.67}$–O–C sample. These observations, together with the corresponding O K-edge measurements of the three bimetallic oxycarbides (not shown), indicate that, among the three bimetallic oxycarbides, the $Nb_{1.0}Mo_{0.67}$–O–C sample is deficient in carbon and rich in oxygen while the $Nb_{1.0}Mo_{2.0}$–O–C sample has a significant amount of graphite at or near the surface region. By comparison, the NEXAFS spectrum of $Nb_{1.0}Mo_{1.75}$–O–C shows only those features that are characteristic of early transition metal oxycarbides in both the C and O K-edge regions. These NEXAFS results are in excellent agreement with the comparative investigations of the catalytic activities of the three catalysts, which indicated that the $Nb_{1.0}Mo_{1.75}$–O–C catalyst has the best hydrodesulfurization (HDS) activity among the Nb–Mo oxycarbide catalysts [34].

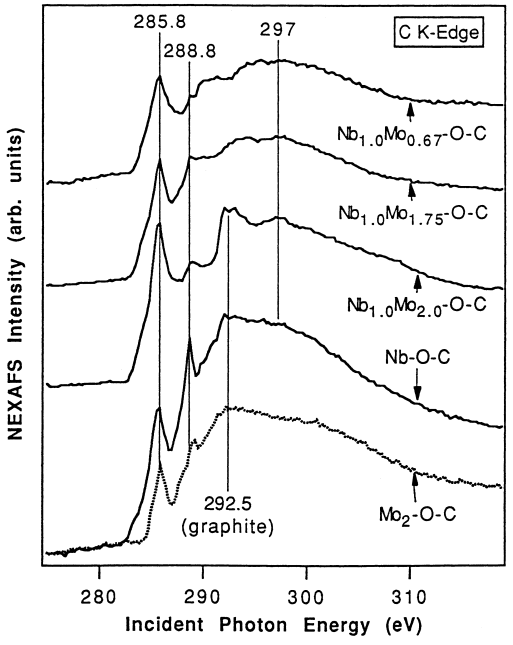

Fig. 7. A comparison of the C K-edge features of three $Nb_{1.0}Mo_x$–O–C bimetallic oxycarbide catalysts with those of the corresponding monometallic oxycarbides. The powder catalysts were synthesized by Oyama et al. [34] using the temperature programmed reaction (TPR) method. The lineshape and the relative intensities of the C K-edge features of the bimetallic oxycarbides are different from those of either monometallic oxycarbides (from [34]).

Fig. 7 also demonstrates that the line shape and the relative peak intensities of the C K-edge features of the Nb–Mo bimetallic oxycarbides, particularly those of the 288.8 eV peak, are different from those of either NbC–O or Mo_2C–O. This observation indicates that the bimetallic oxycarbides do not consist of a simple physical mixture of the two monometallic oxycarbides. Furthermore, since the C K-edge features are

directly related to the *p*-projected DOS of the unoccupied orbitals of the oxycarbides, the differences in the C K-edge features indicate that the electronic properties, and therefore, the catalytic properties, of the Nb–Mo bimetallic oxycarbides should be significantly different from those of either monometallic oxycarbide. This is again in excellent agreement with the comparative investigations of the catalytic activities of the monometallic and bimetallic oxycarbides, which indicated that the HDS activity of the $Nb_{1.0}Mo_{1.75}$–O–C catalyst is better than that of either NbC–O or Mo_2C–O [34].

This so-called synergy effect in bimetallic compounds is also observed in the HDS and HDN activities of bimetallic oxynitride catalysts. For example, the HDS activity of a $V_2MoO_{1.7}N_{2.4}$ bimetallic oxynitride is significantly better than that of either monometallic nitride [35]. NEXAFS studies again provide direct evidence that the electronic properties of $V_2MoO_{1.7}N_{2.4}$ are different from those of either monometallic nitrides. Fig. 8 shows a comparison of the N K-edge spectra of Mo_2N, VN, and $V_2MoO_{1.7}N_{2.4}$ [35]. All three catalysts are characterized by the typical three-peak nitride spectra as discussed for TiN in Fig. 1. A comparison of the three spectra in Fig. 8 clearly shows that the N K-edge spectrum of the V–Mo oxynitride is not from a simple superposition of that of VN and Mo_2N. For example, although the two low energy features of $V_2MoO_{1.7}N_{2.4}$ more closely resemble those of Mo_2N, the peak position and line shape of the high energy feature at 410.5 eV are much more similar to those of VN [35].

The NEXAFS studies of the V–Mo oxynitrides demonstrate that NEXAFS is a very powerful technique for determining the electronic and structural properties of such complicated catalytic systems [35]. The studies of the N and O K-edge spectra provided information about the *p*-projected DOS of the oxynitride and the local bonding environment of the N and O atoms; the measurements of the V L-edge and Mo M-edge features provided additional information about the oxidation states and the DOS of the *d*-orbitals of the two metals. Furthermore, a comparison of the electron yield and fluorescence yield NEXAFS spectra revealed significant differences in the surface and bulk compositions of the $V_2MoO_{1.7}N_{2.4}$ catalyst [35]. For example, the oxidation state is $V^{2.8+}$ for vanadium near the surface region and is $V^{3.8+}$ for vanadium in the bulk. The understanding of these fundamental electronic and structural properties is obviously very critical in achieving an overall understanding of the catalytic properties of this catalyst.

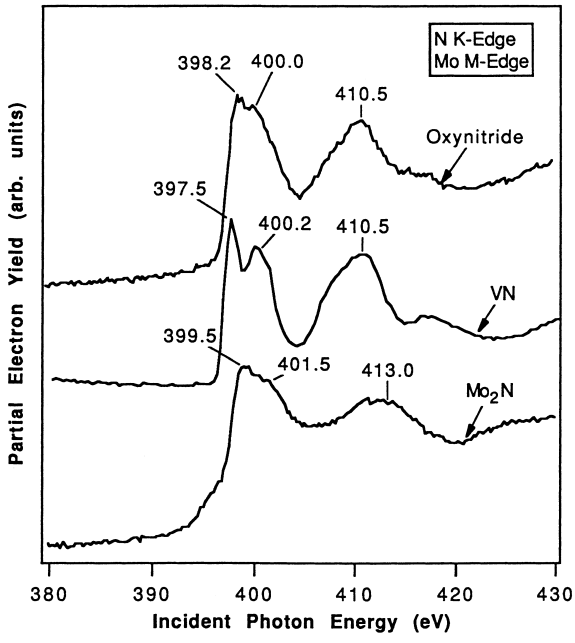

Fig. 8. A comparison of the N K-edge features of a V–Mo bimetallic oxynitride with those of Mo_2N and VN. All samples are in the powder form. The powder catalysts were synthesized by Oyama et al. [35] using the temperature programed reaction (TPR) method. The NEXAFS cross-section for the N K-edge features is much higher than that for the Mo M-edge features; the NEXAFS intensities in Mo_2N and in V–Mo oxynitrides are primarily contributed from N instead of Mo (from [35]).

5.3. *Measurements of S L-edge and O K-edge features*

In addition to measuring the K-edge features of C and N, the NEXAFS technique can also be applied to other 2*p* and 3*p* elements, as discussed in detail in a recent review [9]. For example, Fig. 9 shows the O K-edge features of molybdenum oxides and the S L-edge features of molybdenum sulfides. As compared in the left panel, the O K-edge spectra, in particular the relative intensities of the first two O K-edge features, are very sensitive to the O/Mo stoichiometry such as in MoO_3, MoO_2 and Mo_2C–O. On the other hand, the S L-edge features of transition metal sulfides (TMS) are

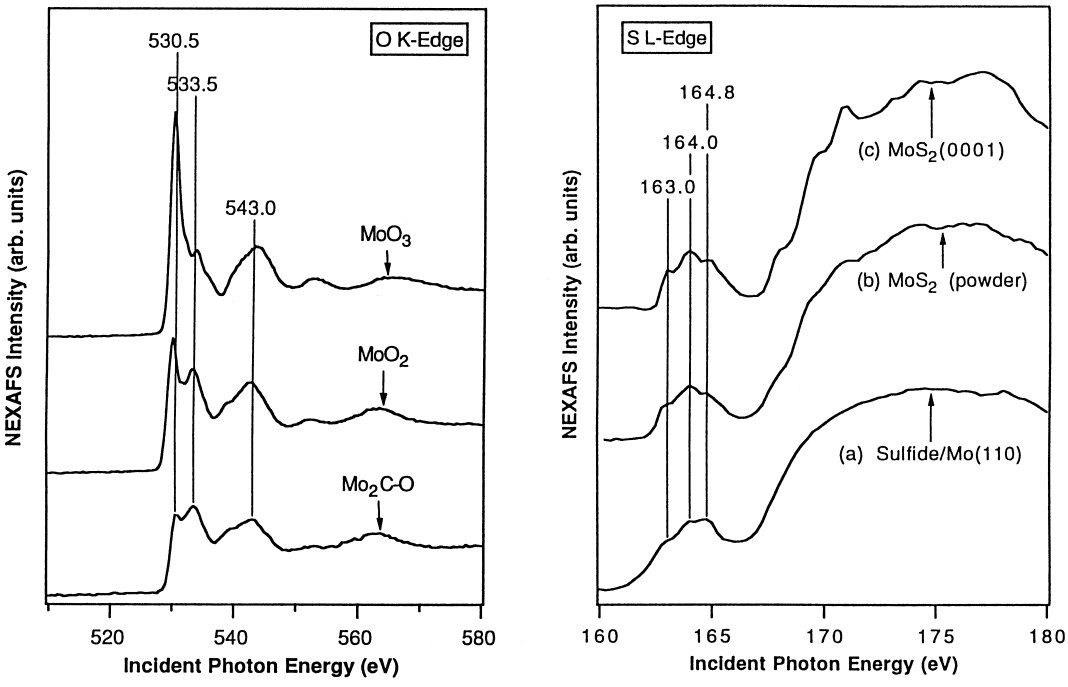

Fig. 9. Left panel: A comparison of the O K-edge spectra of MoO_3, MoO_2, and Mo_2C–O powder materials, which were purchased from Johnson Matthey. Different intensity ratios of the first two K-edge features are related to the different O/Mo stoichiometry in the three catalysts. Right panel: A comparison of the S L-edge features of several MoS_2 samples. The sulfide overlayer on Mo(110) was prepared by reacting Mo(110) with H_2S at 600 K; the MoS_2(0001) bulk crystal was cleaned by a cleavage along the (0001) basal plane prior to the NEXAFS measurements.

extremely sensitive to the crystal structure [9]. As shown in the right panel of Fig. 9, the three S L-edge features at 163.0, 164.0 and 164.8 eV are characteristic for TMS of the layered structure with sulfur atoms in a trigonal prismatic bonding configuration [9]. The S L-edge features in Fig. 9 are qualitatively different from those of TMS of the pyrite structure (e.g. FeS_2), or of the layered structure with sulfur in an octahedral bonding configuration (e.g. TiS_2) [9].

The extreme sensitivity of the NEXAFS technique to the local bonding environment of $2p$ and $3p$ elements makes it a powerful spectroscopy for many future catalytic studies. For example, the O K-edge and S L-edge spectra shown in Fig. 9 would provide the necessary reference NEXAFS data for investigating the HDS mechanism on a Mo_2C–O catalyst. The ability to measure C, O, S, and Mo near edge features would provide detailed information about the fundamental reaction steps and active sites that are responsible for the HDS activity of Mo_2C–O.

Furthermore, a comparison of the S L-edge features in Fig. 9 shows that they are similar for a MoS_2 overlayer prepared on a Mo(110) surface, for amorphous MoS_2 powder materials, and for a bulk MoS_2(0001) single crystal. This similarity again emphasizes the fact that, in the NEXAFS studies of transition metal compounds such as carbides [5,19], nitrides [9], oxides [7,36] and sulfides [9], the NEXAFS spectra of thin overlayers, bulk single crystals, and amorphous powder materials are always very similar as long as they have the same chemical formula.

6. Concluding remarks

In this paper we provided a general overview on the application of NEXAFS for determining the electronic and structural properties of TMC and TMN. We also demonstrated that these electronic and structural prop-

erties are directly related to chemical and catalytic properties. We believe that NEXAFS is one of the most powerful spectroscopies for the investigations of fundamental catalytic properties of TMC and TMN mainly for the following reasons: (1) The NEXAFS spectra provide the DOS of unoccupied orbitals which are directly related to the electronic and structural properties of TMC and TMN. (2) The polarization dependence NEXAFS measurements provide detailed information about the bonding configuration of surface atoms and reaction intermediates on model surfaces, which would lead to the understanding of fundamental catalytic mechanisms. (3) The electron yield and fluorescence yield NEXAFS measurements have substantially different detection limits that can be used to directly differentiate between surface and bulk properties. (4) The NEXAFS technique can be applied equally well to thin overlayers, bulk crystals and amorphous powder materials, which provide the opportunity to directly correlate fundamental studies on model surfaces to powder catalysts.

Acknowledgements

We would like to acknowledge several collaborators who were involved in the measurements of some of the NEXAFS results presented here: Dr. M.L. Colaianni, Mr. B.D. DeVries, Dr. B. Frühberger, Dr. R. Kapoor, Dr. C.-M. Kim, and Dr. S.T. Oyama.

References

[1] R.L. Levy, M. Boudart, Science 181 (1973) 547.
[2] S.T. Oyama, Catal. Today 15 (1992) 179.
[3] S.T. Oyama, The Chemistry of Transition Metal Carbides and Nitrides, Blackie Academic and Professional, Glasgow, 1996.
[4] J.G. Chen, Chem. Rev. 96 (1966) 1477; and references therein.
[5] J.G. Chen, B. Frühberger, J. Eng, Jr., B.E. Bent, J. Mol. Catal. A, in press.
[6] J.G. Chen, D.A. Fischer, J.H. Hardenbergh, R.B. Hall, Surf. Sci. 279 (1992) 13.
[7] J.G. Chen, B.D. DeVries, J.T. Lewandowski, R.B. Hall, Catal. Lett. 23 (1994) 25.
[8] J. Stöhr, NEXAFS Spectroscopy, Springer Series in Surf. Sci. 25, New York, 1992.
[9] J.G. Chen, Surf. Sci. Reports; and references therein, 30 (1997) 1.
[10] D.A. Fischer, J. Colbert, J.L. Gland, Rev. Sci. Instrum. 60 (1989) 1596.
[11] R. Kapoor, S.T. Oyama, B. Frühberger, B.D. DeVries, J.G. Chen, Catal. Lett. 34 (1995) 179.
[12] D.W. Fischer, J. Phys. Chem. Solids 32 (1971) 2455.
[13] F.M.F. de Groot, M. Grioni, J.C. Fuggle, J. Ghijsen, G.A. Sawatzky, H. Petersen, Phys. Rev. B 40 (1989) 5715.
[14] L.A. Grunes, R.D. Leapman, C.N. Wilker, R. Hoffmann, A.B. Kunz, Phys. Rev. B 25 (1982) 7157.
[15] J.G. Chen, B. Frühberger, M.L. Colaianni, J. Vac. Sci. Technol. A 14 (1996) 1668.
[16] J.G. Chen, C.M. Kim, B. Frühberger, B.D. DeVries, M.S. Touvelle, Surf. Sci. 321 (1994) 145.
[17] C.M. Kim, B.D. DeVries, B. Frühberger, J.G. Chen, Surf. Sci. 327 (1995) 81.
[18] J.G. Chen, J. Catal. 154 (1995) 80.
[19] J.G. Chen, B. Frühberger, M.D. Weisel, J.E. Baumgartner, B.D. DeVries, in Ref. [3], p. 439.
[20] B. Frühberger, J.G. Chen, Surf. Sci. 342 (1995) 38.
[21] B. Frühberger, J.G. Chen, J. Am. Chem. Soc. 118 (1996) 11599.
[22] J. Eng, Jr., J.G. Chen, Surf. Sci. in press.
[23] J.G. Chen, B. Frühberger, Surf. Sci. 367 (1996) L102.
[24] J. Eng, Jr., B.E. Bent, B. Frühberger, J.G. Chen, Langmuir 14 (1998) 1301.
[25] J. Eng Jr., B.E. Bent, B. Frühberger, J.G. Chen, J. Phys. Chem. B 101 (1997) 4044.
[26] J.G. Chen, M.D. Weisel, Z.-M. Liu, J.M. White, J. Am. Chem. Soc. 115 (1993) 8875.
[27] J.G. Chen, B.D. DeVries, B. Frühberger, C.M. Kim, Z.-M. Liu, J. Vac. Sci. Technol. A 13 (1995) 1600.
[28] J. Eng, Jr., B.E. Bent, B. Frühberger, J.G. Chen, Catal. Lett. in press.
[29] B. Frühberger, J.G. Chen, J. Eng Jr., B.E. Bent, J. Vac. Sci. Technol. A 14 (1996) 1475.
[30] J. Eng, Jr., B. Frühberger, J.G. Chen, in preparation.
[31] J.G. Chen, M.L. Colaianni, W.H. Weinberg, J.T. Yates Jr., , Chem. Phys. Lett. 177 (1991) 113.
[32] M.L. Colaianni, J.G. Chen, W.H. Weinberg, J.T. Yates Jr., , J. Am. Chem. Soc. 114 (1992) 3735.
[33] B. Dhandapani, S. Ramanathan, C.C. Yu, S.T. Oyama, B. Frühberger, J.G. Chen, J. Catal., in press.
[34] C.C. Yu, S. Ramanathan, B. Dhandapani, J.G. Chen, S.T. Oyama, J. Phys. Chem. B 101 (1997) 512.
[35] R. Kapoor, S.T. Oyama, B. Frühberger, J.G. Chen, J. Phys. Chem. B 101 (1997) 1543.
[36] V.S. Lusvardi, M.A. Barteau, J.G. Chen, J. Eng, Jr., B. Frühberger, A.V. Teplyakov, Surf. Sci. 397 (1998) 237.